## Supporting information

# Proton Trap Effect on Catechol-Pyridine Redox Polymer Nanoparticles as Organic Electrodes for Lithium Batteries

Antonela Galastegui,[a] Daniela Minudri,[a] Nerea Casado,[b] Nicolas Goujon,[b] Fernando Ruipérez,[b] Nagaraj Patil,[c] Christophe Detrembleur,[d] Rebeca Marcilla,[c] David Mecerreyes [b,]*

[a] Instituto de Investigaciones en Tecnologías Energéticas y Materiales Avanzados (IITEMA), Universidad Nacional de Río Cuarto and Consejo Nacional de Investigaciones Científicas y Tecnológicas (CONICET), Campus Universitario, 5800 Río Cuarto, Argentina.

[b] POLYMAT University of the Basque Country UPV/EHU, Av. Tolosa 72, 20018, San Sebastian, Spain.

[c] Electrochemical Processes Unit, IMDEA Energy, Avenida Ramón de la Sagra 3, 28935 Móstoles, Madrid, Spain.

[d] Centre for Education and Research on Macromolecules (CERM), CESAM Research Unit, University of Liege, Allée de la Chimie B6A, 4000 Liège, Belgium.

## Synthesis of DMA

Dopamine methacrylamide (DMA) was synthesized employing the next reagents: dopamine hydrochloride was purchased from Alfa Aesar; triethylamine, methacryloyl chloride, NaCl and $MgSO_4$ were obtained from Sigma Aldrich; methanol, HCl and ethyl acetate were purchased from Acros.

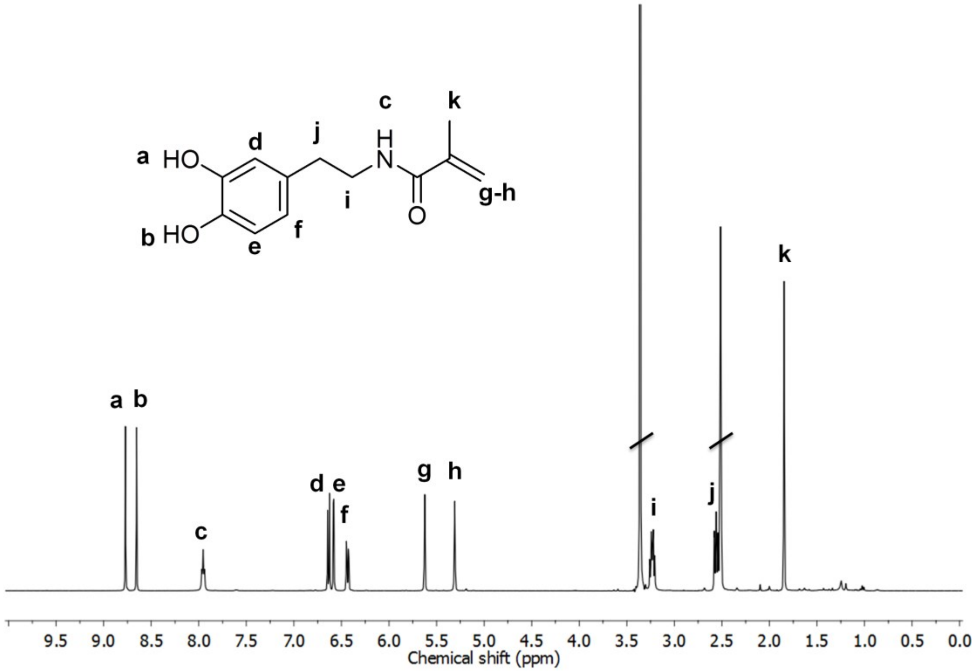

**Figure S1**. $^1H$ NMR spectrum of dopamine methacrylamide (DMA) in DMSO-$d_6$. The crossed out peaks belong to the solvent employed for the technique, DMSO-$d_6$.

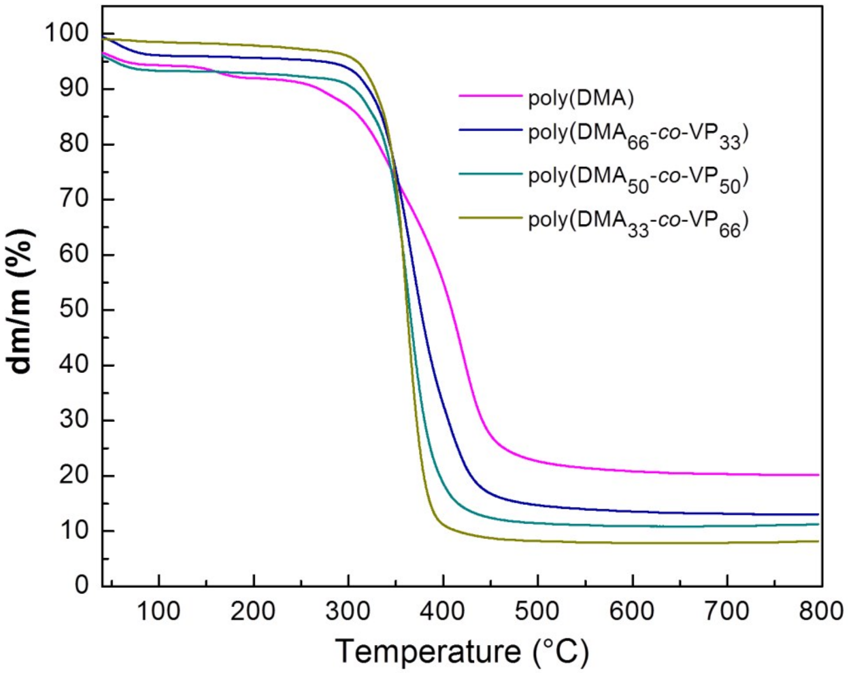

**Figure S2.** Thermal behavior of the RPNs by TGA.

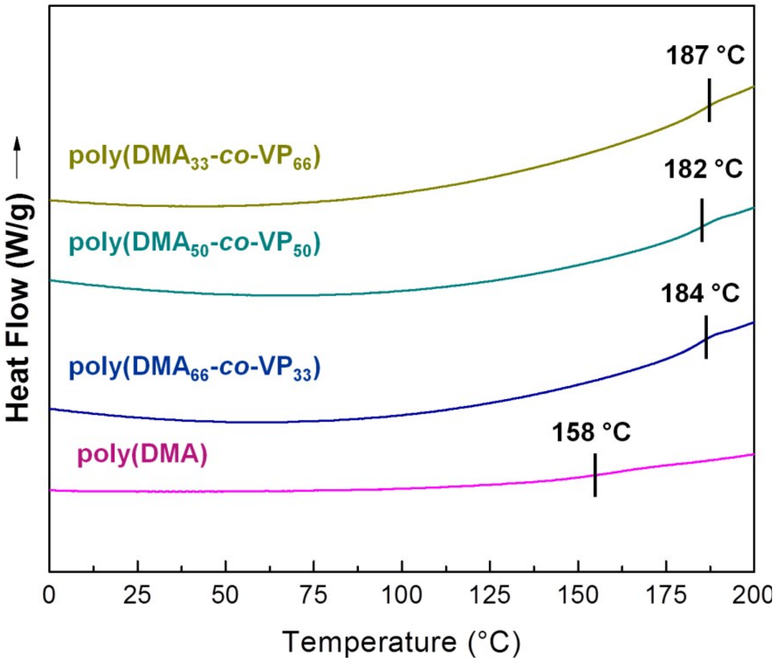

**Figure S3.** Thermal behavior of the RPNs by DSC.

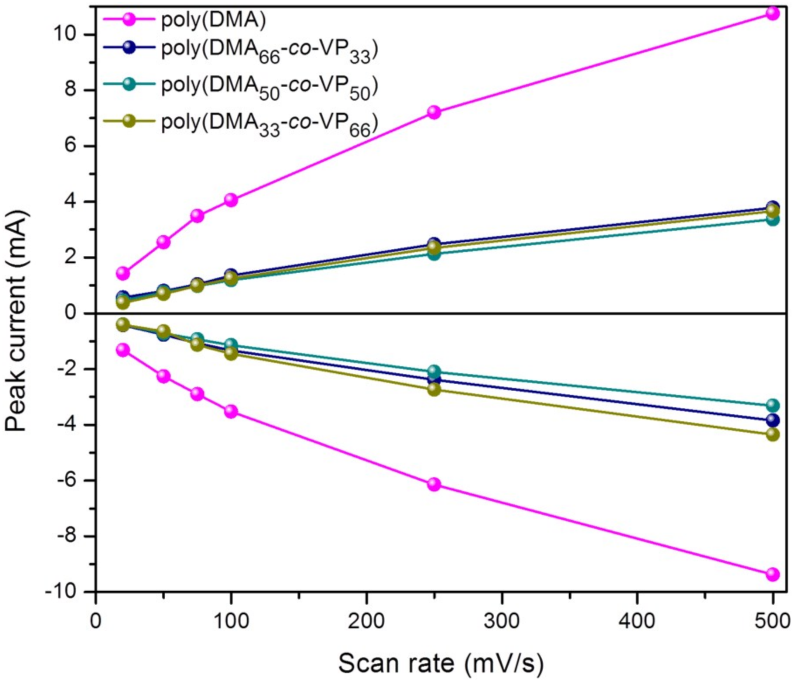

**Figure S4.** Scan rate study at 0.1 M $HClO_4$ varying the scan rate between 20 and 500 mV/s.

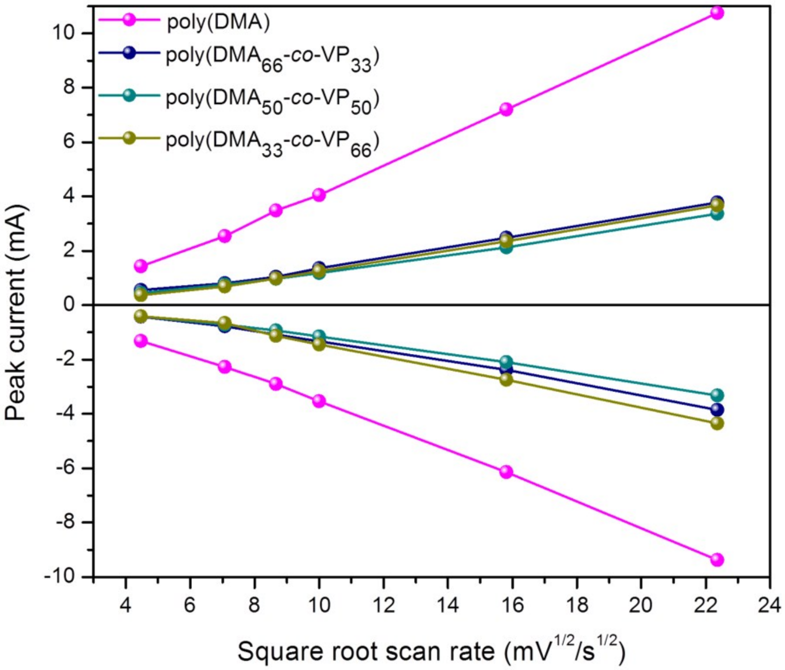

**Figure S5.** Maximum cathodic ($I_c$) and anodic ($I_a$) current vs square root scan rate for all the nanoparticles in acidic media.

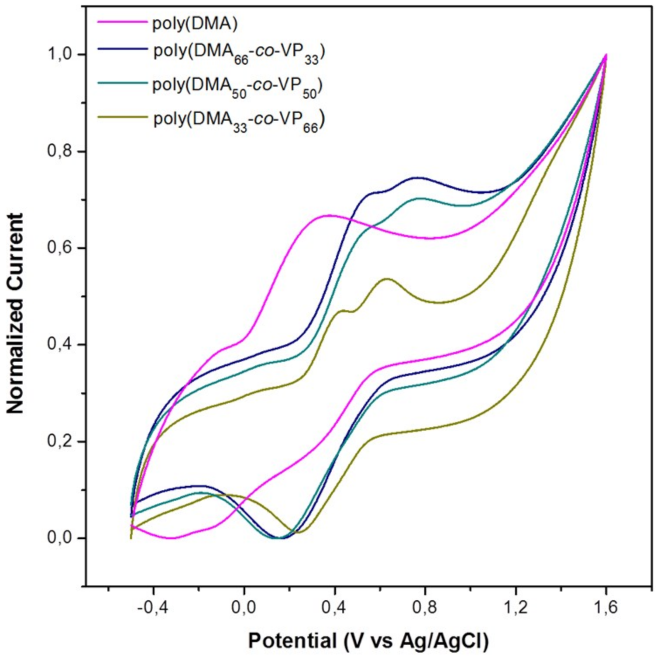

**Figure S6.** Cyclic voltammetry of redox active catechol-pyridine nanoparticles at 20mV/s in aqueous electrolyte (0.1 M - LiTFSI).

In Figure S6 as well as Figure 4a, corresponding to electrochemical studies in organic and aqueous media respectively, the third cycle is shown for all nanoparticles since the catechol RPN has a particular behavior. They present first irreversible oxidation peaks (or activation peaks) that disappear after the second cycle. This performance is due to the change of $H^+$ by $Li^+$ cation in the catechol structure, the equilibrium between hydroquinone lithium salt/Quinone appear as a reversible redox process at lower potential values due to negative charge on the oxygen. This performance of RPNs was previously reported in the literature (N. Patil, A. Mavrandonakis, C. Jérôme, C. Detrembleur, J. Palma and R. Marcilla, *ACS Appl. Energy Mater.*, 2019, **2**, 3035–3041; K. Pirnat, N. Casado, L. Porcarelli, N. Ballard and D. Mecerreyes, *Macromolecules*, 2019, **52**, 8155–8166).

.

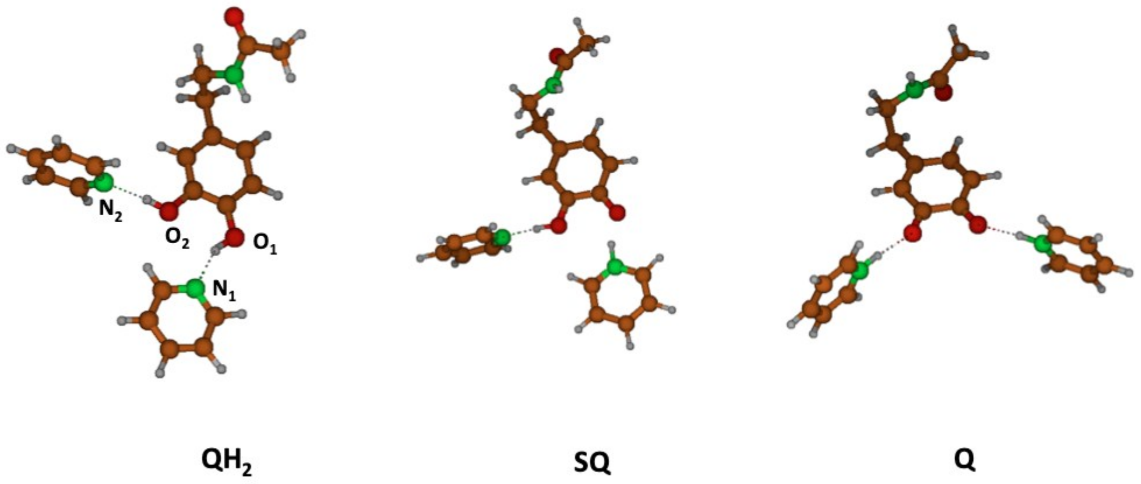

**Figure S7.** Molecular structures of the hydroquinone ($QH_2$), semiquinone (SQ) and quinone (Q).

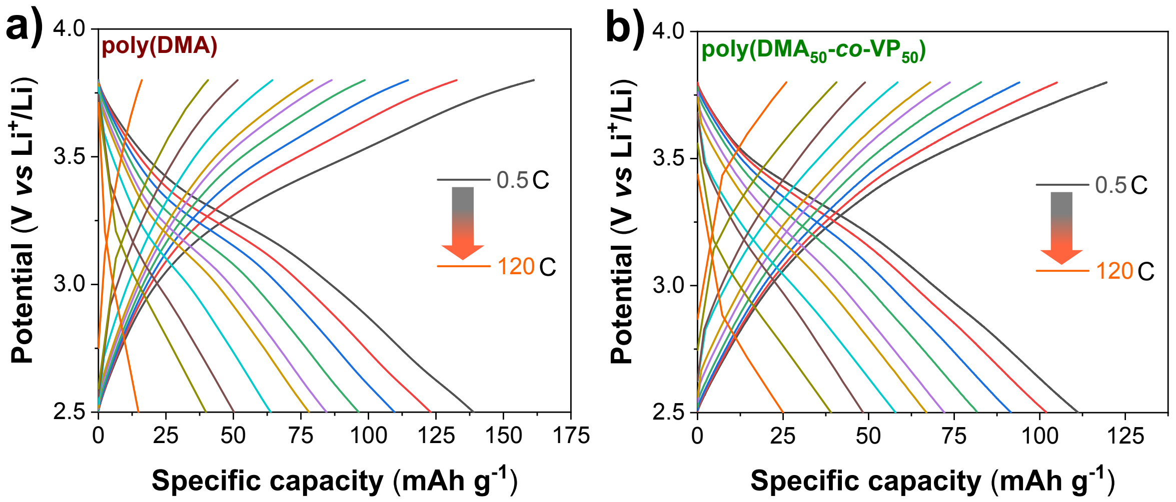

**Figure S8.** Representative galvanostatic specific capacity–potential profiles at various C-rates for poly(DMA) (a), and poly($DMA_{50}$-*co*-$VP_{50}$) (b) in Li-ion half-cell configuration.

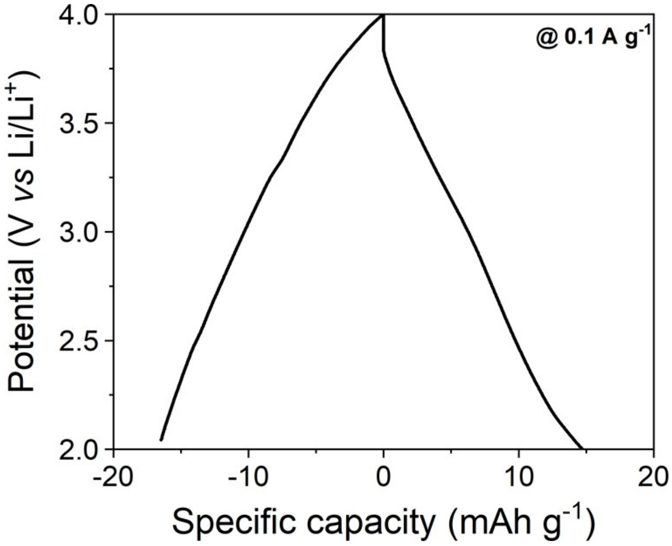

**Figure S9.** Galvanostatic specific capacity–potential profiles at 0.1 A g$^{-1}$ for CNT blank electrode in Li-ion half-cell configuration. Positive electrode: CNTs/PVDF (70/30 wt%) deposited on carbon paper. Negative electrode: Li foil.

In order to evaluate double-layer contribution of CNTs to the total capacity of composite electrode, CNT blank electrode was measured through GCD experiment (Figure S9). Under the similar experimental conditions, the capacity contribution of this blank electrode was only ~15 mAh g$^{-1}$.

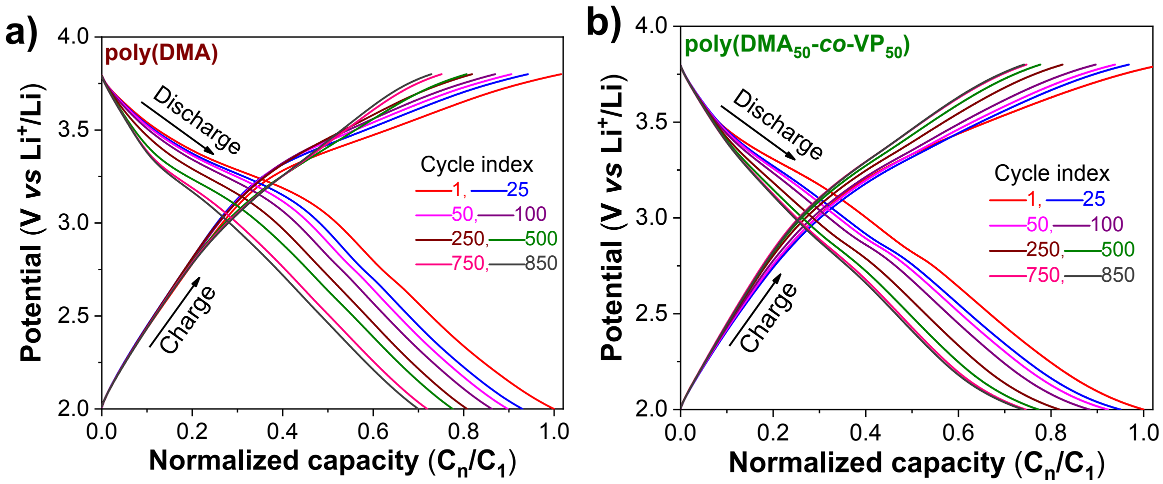

**Figure S10.** Representative galvanostatic specific capacity–potential profiles at different cycle indexes for poly(DMA) (a), and poly(DMA$_{50}$-*co*-VP$_{50}$) (b) in Li-ion half-cell configuration.